Available online at www.sciencedirect.com
ScienceDirect
Geochimica et Cosmochimica Acta 73 (2009) 2712–2726
Geochimica et Cosmochimica Acta
www.elsevier.com/locate/gca

Diffusion of ionic tracers in the Callovo-Oxfordian clay-rock using the Donnan equilibrium model and the formation factor

D. Jougnot [a,b,c,*], A. Revil [b,c], P. Leroy [d]

[a] ANDRA, 1-7 rue Jean Monnet, 92298 Châtenay-Malabry, France
[b] CNRS-UMR 5559-LGIT, Université de Savoie, Equipe volcan, 73376 Le-Bourget-du-Lac, France
[c] Colorado School of Mines, Green Center, Department of Geophysics, 1500 Illinois Street, Golden, CO 80401, USA
[d] BRGM, 3 avenue C. Guillemin, BP 6009, 45061 Orléans, France

Received 4 August 2008; accepted in revised form 21 January 2009; available online 5 March 2009

Abstract

The transient diffusion of cationic and anionic tracers through clay-rocks is usually modeled with parameters like porosity, tortuosity (and/or constrictivity), sorption coefficients, and anionic exclusion. Recently, a new pore scale model has been developed by Revil and Linde [Revil A. and Linde N. (2006) Chemico-electromechanical coupling in microporous media. *J. Colloid Interface Sci.* **302**, 682–694]. This model is based on a volume-averaging approach of the Nernst–Planck equation. The influence of the electrical diffuse layer is accounted for by a generalized Donnan equilibrium model through the whole connected pore space that is valid for a multicomponent electrolyte. This new model can be used to determine the composition of the pore water of the Callovo-Oxfordian clay-rock, the osmotic efficiency of bentonite as a function of salinity, the osmotic pressure, and the streaming potential coupling coefficient of clay-rocks. This pore scale model is used here to model the transient diffusion of ionic tracers ($^{22}Na^{+}$, $^{36}Cl^{-}$, and $^{35}SO_4^{2-}$) through the Callovo-Oxfordian clay-rock. Speciation of SO_4^{2-} shows that ~1/3 of the SO_4 is tied-up in different complexes. Some of these complexes are neutral and are therefore only influence by the tortuosity of the pore space. Using experimental data from the literature, we show that all the parameters required to model the flux of ionic tracers (especially the mean electrical potential of the pore space and the formation factor) are in agreement with independent evaluations of these parameters using the osmotic pressure determined from in situ pressure measurements and HTO diffusion experiments.

1. INTRODUCTION

The diffusion of ions in charged porous media like clay materials has been studied by a number of researchers for a variety of geoenvironmental applications including ground water contamination from clay-lined landfills (Malusis et al., 2003) and the spreading of contaminants from canisters containing nuclear wastes (Chatterji, 2004). The possibility to use clay-rocks as a potential host for the long-term isolation of nuclear wastes has recently driven new researches in this field. The French Nuclear Waste Agency (ANDRA) is presently studying the long-term storage of high-level long-lived nuclear wastes in the Callovo-Oxfordian (COx) clay-rock formation in the eastern part of the Paris basin (ANDRA, 2005). The COx clay-rock is composed of clay-minerals (between 20% and 50% by weight), silica, and carbonates. Because of the low intrinsic permeability of this formation (in the range 10^{-19}–10^{-21} m^2, Escoffier et al., 2000; Gasc-Barbier et al., 2004), diffusion of ions is considered to be the major mechanism of the potential spread of ionic species both in the medium (Cey et al., 2001; Patriarche et al., 2004).

To understand the diffusion of ions in such a complex material, new experiments were performed recently to evaluate the diffusion and the sorption of radio-isotopic elements

* Corresponding author.
E-mail address: djougnot@mines.edu (D. Jougnot).

0016-7037/$ - see front matter © 2009 Elsevier Ltd. All rights reserved.
doi:10.1016/j.gca.2009.01.035

(Melkior et al., 2004, 2005, 2007; Bazer-Bachi et al., 2005, 2007 and references therein). However, these authors used phenomenological models and empirical parameters to explain why the intrinsic diffusion coefficient of some sorbed cationic species (like Na^+, K^+, or Cs^+) are higher than the diffusion coefficient of anions (e.g., chloride). Their approach does not take into account explicitly the influence of the microstructure and electrochemical properties of the mineral/water interface on the diffusivity of ions and long-term range force like the Coulomb force (Revil, 1999).

Recently, Appelo and Wersin (2007) used a generalized Donnan equilibrium model to include the effect of the diffuse layer at the mineral/water interface of clay materials upon the diffusivity of ionic species. However, their model does not consider the existence of the Stern layer where most of the charged counterions are located (Leroy and Revil, 2004; Leroy et al., 2007, 2008).

In this paper, we are interested to test the approach developed recently by Revil and Linde (2006), Leroy et al. (2006), and Revil (2007). Revil and Linde (2006) and Revil (2007) developed a unifying model of transport properties of water and ions in charged microporous materials. This model is obtained by upscaling the local constitutive equations (Nernst–Planck and Navier–Stokes equations) using a volume-averaging operator. Consequently, the constitutive equations established some simple, and theoretically-based, relationships between the measurable material properties, the key-microstructural parameters of the porous medium (formation factor and intrinsic permeability), and the electrochemical properties of the double layer coating the clay particles. This model was recently extended to include the effect of partial saturation upon electrokinetic properties (Linde et al., 2007; Revil et al., 2007) and the diffusion of ions in a concentration field for partially saturated media (Revil and Jougnot, 2008). Leroy et al. (2007) have also modeled the composition of the pore water of the Callovo-Oxfordian clay-rock using an extension of this model by dividing the porosity into two compartments depending on the pore size distribution and the thickness of the diffuse layer.

In the present paper, we adapt this modeling approach in order to study the diffusion of radio-active tracers in a clay-rock. Because the pore size distributions of the samples investigated in the present study are unknown, we use a Donnan model for which the homogenization volume is the whole connected pore space and not only the fraction of the pores affected by the diffuse layer. This approach is consistent with the original Donnan approach (Teorell, 1935; Meyer and Sievers, 1936) which has been generalized by Revil and Linde (2006). After a rapid review of the classical diffusion models used in the literature to interpret such type of data, we present the microscopic description and underlying assumptions of our tracer diffusion model. This model is tested against recent experimental data using a variety of three radio-active tracers ($^{22}Na^+$, $^{36}Cl^-$, and $^{35}SO_4^{2-}$) on different samples of the Callovo-Oxfordian clay-rock in the porosity range 0.03–0.15. The models show also a consistency between the mean electrical potential existing in the pore space of the clay-rock and the electrical potential needed to explain the osmotic pressure in the COx formation.

2. STATE OF THE ART

The diffusion of ions through a porous material is classically based on the Fick constitutive equation. The flux of the species i through a porous material, $\mathbf{J}_i$ (in mol m^{-2} s^{-1}) is usually described by the Fick's first law,

$$\mathbf{J}_i = -D_i \nabla C_i, \tag{1}$$

where D_i is the effective diffusion coefficient in the medium (in m^2 s^{-1}) and C_i the concentration of species i in the porous medium (in mol m^{-3}). The concentrations, usually expressed in mol L^{-1}, are expressed below in m^{-3} in the metric system.

Several models have been developed to express D_i in terms of the textural properties of the porous material (see Bourg et al., 2003; Bourg, 2004 for some phenomenological models and Melkior et al., 2007 for a short review of the literature). It is notoriously known that porosity cannot be used alone to determine the diffusion coefficient. Tortuosity is used to account for the tortuous path of the ions during their migration through the pore space and constrictivity to account for the fact that only a fraction of the porosity is used as a pathway for the diffusion of the ions. One of the most popular models to account for tortuosity was developed by Van Brakel and Heertjes (1974). It yields,

$$D_i = \phi D_i^f \frac{\delta}{\tau^2}, \tag{2}$$

where D_i^f (in m^2 s^{-1}) is the self-diffusion coefficient of species i in the bulk pore water, ϕ is the total connected porosity, τ is the tortuosity of the bulk pore space, and δ is the constrictivity. Further in this paper, we will propose to distinguish two components in the constrictivity parameter: a geometrical constrictivity (δ_g) for the pore space topography and an electrostatic constrictivity (δ_{el}) for the electrostatic interactions between ions and charged mineral surfaces.

The continuity equation for the species i, in a porous medium, can be expressed by the Fick's second law:

$$\phi \frac{\partial C_i}{\partial t} + (1-\phi)\rho_g \frac{\partial C_i^S}{\partial t} = -\nabla \cdot \mathbf{J}_i, \tag{3}$$

with C_i^S the concentration of ions i that are sorbed onto the mineral surface (in mol kg^{-1}), ρ_g the grain density (in kg m^{-3}), and t the time (in s). The second term of the left hand side of Eq. (3) corresponds to a source/sink term that is associated with the interactions of the solution with the surface of the minerals. Sorption of solutes in a porous medium can be represented by simple isotherms (see Limousin et al., 2007 for a recent review) or models accounting for electrical double or triple layer theory (Leroy and Revil, 2004; Leroy et al., 2007) assuming or not instantaneous and reversible adsorption. Assuming that the ratio between the sorbed concentration and solution concentration is constant with time, it is customary to introduce a distribution or partitioning coefficient defined by $K_d^i = C_i^S / C_i$ (in m^3 kg^{-1}) (e.g., Limousin et al., 2007). Using this definition, Eq. (3) can be written as follow:

$$\left[\phi + (1-\phi)\rho_g K_d^i\right] \frac{\partial C_i}{\partial t} = -\nabla \cdot \mathbf{J}_i, \tag{4}$$

where $[\phi + (1-\phi)\rho_g K_d^i]$ is equivalent to ϕR_d^i, where R_d^i is the well-known retardation factor. Introducing the effective sorption and the Fick's first law in Eq. (4) yields the classical diffusion equation,

$$\frac{\partial C_i}{\partial t} = \nabla \cdot (\eta_i \nabla C_i), \tag{5}$$

where η_i, the apparent diffusivity of ion i, is defined by,

$$\eta_i = \frac{D_i}{[\phi + (1-\phi)\rho_g K_d^i]}. \tag{6}$$

In Eq. (6), K_d^i is sometimes used as a constant. However, it is rare that sorption can be represented by "simple isotherms", which have mostly been shown not to work at all when any kind of competition is at play (either from strong aqueous complexes, as in the case of uranium and carbonate, or from other sorbed species, given a finite sorption capacity) (Zachara et al., 2002; Steefel et al., 2003, 2005; Zhu, 2003).

Note that in this paper, we use the expression "diffusion coefficient" to describe the material properties arising in Fick's first law (which is the constitutive equation) and the term "diffusivity" to describe the material properties arising in the diffusion equation obtained by combining Fick's first and second laws. If sorption can be neglected for a given tracer, the diffusivity of this tracer is equal to the ratio between the effective diffusion coefficient and the porosity $\eta_i = D_i/\phi$ (Revil and Leroy, 2004; Revil et al., 2005).

The previous model is however too simplistic. It does not account for the influence of the electrical diffuse layer (e.g., Appelo et al., 2008). To account for this effect, Muurinen et al. (1988) proposed the introduction of an effective porosity ϕ_{eff} in the mass conservation equation. This yields:

$$\phi_{eff_i} \frac{\partial C_i}{\partial t} = \nabla \cdot \left(\frac{\phi_{eff_i} D_i^f}{\tau^2} \nabla C_i \right). \tag{7}$$

For anions, this effective porosity can also be modeled by using a negative value of the distribution coefficient. This very popular approach is however phenomenological in nature and ϕ_{eff} is a fitting parameter that takes different values for different ions.

Bourg (2004) and Bourg et al. (2006) proposed a diffusion model in bentonite. This model divides the medium in three parallel pore networks: a macroporous one and two microporous (a two-layer and a three-layer water molecule in the clay interlayer porosity both corresponding to the so-called bound water). Due to their negative charge, this model considers that anions have no access to the two last microporous network. Each pore diffusion is described with a tortuosity τ (considered as a geometrical parameter) and a constrictivity δ (which take into account pore section variability, steric effect, and viscosity effect). In addition, Bourg (2004) considered the same tortuosity for the three networks. The total diffusion flux is the sum of the fluxes for each pore network.

Other authors consider the division of the connected porosity into compartments: one for the sorbed species and/or the diffuse layer and the other for the free water (Appelo et al., 2008). According to Kim et al. (1993) and Eriksen et al. (1999), these two compartments contain mobile charges. Therefore two diffusion coefficients have to be considered: the bulk diffusion coefficient D_i and the surface diffusion coefficient D_i^S (in $m^2\ s^{-1}$). Introducing this surface diffusion coefficient in the constitutive equation yields,

$$\mathbf{J}_i = -\left[D_i + (1-\phi)\rho_g K_d^i D_i^S\right] \nabla C_i. \tag{8}$$

This model was used by Muurinen (1994) to model the diffusion of cations in charged porous media. He found that D_i is generally stronger than D_i^S by at least one order of magnitude. This result is consistent with the fact that the electromigration mobility of the counterions in the Stern layer is usually smaller than the mobility of the ions in the bulk pore water by one order of magnitude (Revil et al., 1998; Revil, 1999). However, there is no reason that surface diffusion would act in parallel to the bulk diffusion. We know, from electrical conductivity models, that the electromigration of the ions follows very different paths between the bulk pore space and the surface of the pores (Bernabé and Revil, 1995; Revil et al., 1998; Revil, 1999). In addition, there is no clear picture of surface diffusion in the Stern layer. Models for the electromigration of the counterions in the Stern layer predict no migration of the counterions in this layer at zero frequency (Leroy et al., 2008; Leroy and Revil, 2008, submitted to Journal of Geophysical Research, 2008). Because of the intrinsic connection between diffusion and electromigration, this implies that the diffusion of the counterions in the Stern layer is physically not possible because it is not possible to build surfaces concentrations/activity gradients in the Stern layer. In addition, the fraction of counterions between the Stern layer and the diffuse layer is relatively independent of the salinity of the pore water for the salinity range considered in this paper (see Leroy and Revil, 2004). Recent modeling of the effect of the salinity upon the partition coefficient of the counterions between the Stern and the diffuse layers (Leroy and Revil, submitted to Journal of Geophysical Research, 2008) shows that the partition coefficient increases slightly with the salinity in agreement with the fact that the diffuse layer disappears at $I \sim 0.2$ M.

The main problem with the previous approaches is that they do not take into consideration the influence of the electrical diffuse layer upon the concentrations of the ionic species in the pore space of the clay-rock (see Leroy et al., 2007). Some diffusion models, however, are partially based on the properties of the electrical double layer. Several authors have proposed to divide the pore space into three compartments (i) the Stern layer with immobile sorbed ions, (ii) the diffuse layer with mobile ions (but with concentrations determined by solving the Poisson-Boltzmann differential equation), and (iii) the bulk water of the pore which contains free ions. Sato et al. (1995) proposed for example to introduce the contribution of ion located in the diffuse double layer with an electrostatic constrictivity δ_{el}:

$$\mathbf{J}_i = -\delta_{el} D_i \nabla C_i. \tag{9}$$

This electrostatic constrictivity is the ratio between the average concentration of ion in the diffuse layer $C_i^d(x)$ and the concentration in the bulk water C_i (Sato et al., 1995),

$$\delta_{el} = \frac{1}{RC_i} \int_0^R C_i^d(x) dx, \tag{10}$$

where R is the mean pore radius, x is the distance normal to the surface of the pores, and $C_i^d(x)$ is the local concentration of species i determined by solving the Poisson-Boltzmann equation at the microscale. Ochs et al. (2001) used however electrostatic constrictivity as a fitting parameter, so their approach remains limited. We will show in Section 3 that our approach yields a better expression to determine the electrostatic constrictivity, which will be based on an extension of Donnan equilibrium theory.

Molera and Eriksen (2002) use a partition coefficient f between the species located in the diffuse layer and those located in the Stern layer. This fraction is assumed to have no dependence with C_i and C_i^S. This yields another expression for the constitutive equation,

$$\mathbf{J}_i = -\left\{ D_i \left[1 + f \frac{(1-\phi)}{\phi} \rho_g K_d^i \right] \right\} \nabla C_i. \tag{11}$$

However, they do not provide a way to estimate this parameter from the underlying electrical double layer theory. We will show below that our model is able to determine the value of this parameter.

In all the models discussed previously, the parameters involved in the generalized Fick's law (like the electrostatic constrictivity δ_{el} or the coefficient f) have to be determined empirically. In the next section, we use a ionic diffusion model based on a volume-averaging approach of the Nernst–Planck equation and related to the electrical double layer theory (Revil and Linde, 2006).

3. A NEW MODEL

When dealing with a general strategy to upscale local constitutive equations in a charged porous medium, there are two main avenues. The former consists in simplifying the topology of the pore network by assuming a simple geometry. For example, the pore network can be assumed to be made of a set of capillaries with a known pore size distribution, a given local or macroscopic tortuosity, and possibly some connectivity described by percolation theory. In this case, it is possible to solve exactly the Poisson-Boltzmann equation for each capillary and to determine the effective properties at the scale of a representative elementary volume. This requires that this simplification of the geometry is a good assumption and that the pore size distribution is known.

A second avenue consists in performing an homogenization of the diffuse layer plus the free water at the local scale (replacing the Poisson-Boltzmann problem by the Donnan problem, Teorell, 1935; Meyer and Sievers, 1936) and upscaling the local solution at the macroscopic scale using for example a volume-averaging approach (Revil and Linde, 2006). This has the advantage of using less restrictive assumptions regarding the geometry of the porous material and discussing the effect of the microgeometry using effective parameters like the formation factor for instance. Following Revil and Linde (2006), we use this second approach below.

3.1. Underlying assumptions

The Callovo-Oxfordian (COx) clay-rock (Fig. 1) is a complex material with both micropores and macropores.

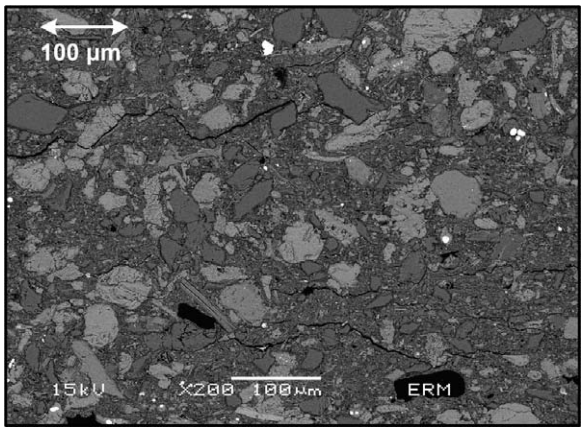

Fig. 1. Picture of a COx sample by scanning electron microscopy (credit: J.C. Robinet). The silica and carbonate grains are embedded into a clay matrix.

The distinction between these two families of pores is based on the thickness of the diffuse layer, which depends in turn of the ionic strength of the solution in equilibrium locally with the medium. We will consider below Donnan equilibrium over the full connected porosity as done classically with the Donnan model. The reason is that usually the pore size distribution is not available to apply the more sophisticated model developed recently by Leroy et al. (2007).

The COx clay-rock is considered to be a charged porous medium fully saturated by a multicomponent electrolyte with Q species. The surface of the solid phase of the clay particles is assumed to carry a net electrical charge density because of the complexation of the surface sites with the elements of the pore water and isomorphic substitution in the crystalline framework of smectite. This surface charge density is responsible for the formation of an electrical triple layer (Fig. 2) that includes the Stern layer and the diffuse layer (e.g., Hunter, 1981).

The electroneutrality of a representative elementary volume of the clay-rock is written as (Revil and Linde, 2006):

$$\overline{Q}_V + \frac{S}{V_f} Q_S = 0, \tag{12}$$

where $\overline{Q}_V$ is the total charge of the diffuse layer per unit pore volume of the connected porosity, $Q_S = Q_0 + Q_\beta$ is the total (fixed) surface charge density (in C m^{-2}) on the surface of the clay particles. This charge density includes the charge density due to the active sites covering its surface Q_0 and the charge density of the Stern layer Q_β (Fig. 2). In Eq. (12), S (in m^2) is the surface area of the interface separating the solid and the liquid phases in a representative elementary volume of the material, and V_f is the pore volume (in m^3) of the same representative elementary volume. The volumetric charge density $\overline{Q}_V$ corresponds to the net amount of charge of the diffuse layer per unit pore volume (in C m^{-3}). It is defined by:

$$\overline{Q}_V = (1 - f_Q) Q_V, \tag{13}$$

where f_Q is the fraction of charge carried by the counterions located in the Stern layer or, in other words, the partition coefficient of the countercharge between the Stern and the

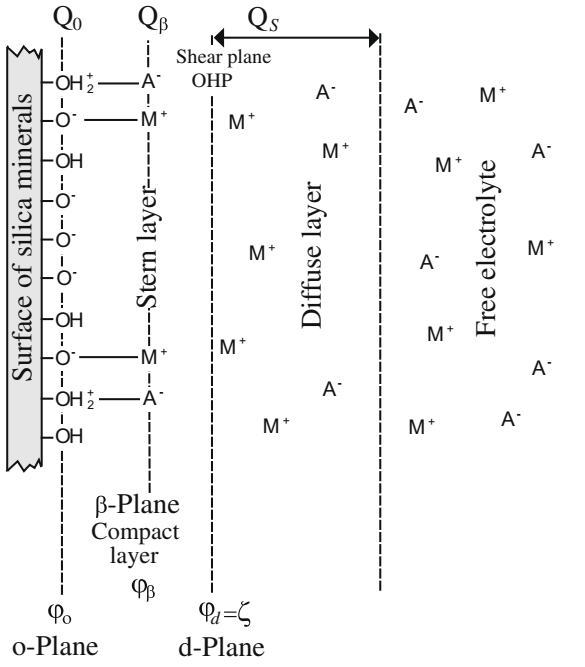

Fig. 2. Sketch of the electrical triple layer extending from the surface of the clay minerals to the center of the pore. M^+ represents metal cations and A^- the anions.

diffuse layers, and Q_V represents the total charge density associated with the cation exchange capacity of the material (Revil et al., 2002)

$$Q_V = \rho_g \left(\frac{1-\phi}{\phi}\right) CEC, \tag{14}$$

where ρ_g represents the solid grain density (in kg m^{-3}) and the CEC is the cation exchange capacity of the medium (in mol kg^{-1}). Using an electrical triple layer model, Leroy et al. (2007) obtained $f_Q = 0.94 \pm 0.02$ at 25 °C for the COx clay-rock. Gonçalvès et al. (2007) obtained $f_Q \propto 0.85$ from filtration efficiency experimental data for a compacted bentonite. Leroy and Revil (submitted to Journal of Geophysical Research, 2008) obtain for smectite f_Q in the range 0.85–0.90 using a TLM model. In all cases, this means that a large fraction of the counterions are located in the Stern layer.

In thermodynamic equilibrium, the Donnan equilibrium model is based on the equality between the electrochemical potential of the ions in the pore space of the charged porous material and in a reservoir of ions in contact with the charged porous material. In terms of concentrations, the concentration of the species i in the pore space of the material, $\overline{C}_i$, is related to the concentration of the species i in the reservoir, C_i, by (e.g., Leroy et al., 2007)

$$\overline{C}_i = C_i \frac{\gamma_i}{\bar{\gamma}_i} \exp\left(-\frac{q_i \varphi_m}{k_B T}\right), \tag{15}$$

where $q_i = (\pm e) z_i$ represents the charge of the ion i (in C) with z_i the charge number of the ion and e the elementary charge (1.6×10^{-19} C), k_B the Boltzmann constant (1.381×10^{-23} J K^{-1}), T the absolute temperature in K, γ_i and $\bar{\gamma}_i$ are the activity coefficients of ion i in a reservoir of ions in local equilibrium with the porous material and in the pore space of the COx clay-rock, respectively, and φ_m is the mean electrical potential in the pore space of the medium. Leroy et al. (2007) showed that, at the ionic strength of the bulk pore water, the ratio of the activity coefficients can be neglected ($\gamma_i/\bar{\gamma}_i \approx 1$).

The potential φ_m can be determined from the volumetric charge density $\overline{Q}_V$ by solving numerically the following charge balance equation (see Revil and Linde, 2006; Leroy et al., 2007),

$$\overline{Q}_V = \sum_{i=1}^{Q} q_i C_i \exp\left(-\frac{q_i \varphi_m}{k_B T}\right). \tag{16}$$

To perform these computations, we need the macropore water composition proposed for example by the THERMOAR model (Gaucher et al., 2006) at 25 °C. Following Leroy et al. (2007), we took CEC = 0.18 mol kg^{-1}, $\rho_g = 2700$ kg m^{-3}, $T = 298.15$ K (25 °C), and $f_Q = 0.94 \pm 0.02$. With these parameters, we will show later that the mean electrical potential of the entire pore space of the COx clay-rock is typically in the range from −15 to −40 mV.

From Eqs. (10) and (15) and using $\gamma_i/\bar{\gamma}_i \approx 1$, the mean electrical potential can be also related to the electrostatic constrictivity introduced by Sato et al. (1995) (see Section 2):

$$\delta_{el} = \frac{\overline{C}_i}{C_i} = \exp\left(-\frac{q_i \varphi_m}{k_B T}\right). \tag{17}$$

For the COx clay-rock, surface properties are dominated by the reactivity and specific surface area of smectite. Using a triple layer model, we determined the distribution coefficient $K_d^i = C_i^S / C_i$ using the calculated surface site density of sorbed counterions in the Stern layer Γ^0_{Xi}(in sites m^{-2}). The subscript "X" refers here to the surface sites resulting from isomorphic substitutions into the mineral lattice and situated on the basal planes of the smectite particles (Leroy et al., 2007). In most of experimental studies, the distribution coefficient K_d^i is obtained by batch or column experiment for each type of tracer.

The concentration of sorbed species C_i^S is given by:

$$C_i^S = \Gamma^0_{Xi} S_{sp}, \tag{18}$$

where S_{sp} is the specific surface area (in m^2 kg^{-1} of mineral). Gaucher et al. (2004) proposed an average value of the specific surface for the COx: $S_{sp} = 5 \times 10^4$ m^2 kg^{-1}. In the case of monovalent and bivalent counterions, respectively, the surface site density of sorbed counterions in the Stern layer Γ^0_{Xi} is determined by Leroy et al. (2007):

$$\Gamma^0_{Xi} = \frac{\Gamma^0_X a_i}{K_i} \exp\left(-\frac{e\varphi_\beta}{k_B T}\right), \tag{19}$$

$$\Gamma^0_{Xi} = -\frac{e{\Gamma^0_X}^2 a_i}{2K_i Q_0} \exp\left(-\frac{2e\varphi_\beta}{k_B T}\right), \tag{20}$$

where φ_β is the electrical potential at the Stern plane and Γ^0_X the total surface site density of the "X" sites. Using the model of Leroy et al. (2007), we determined an average of these two parameters for the COx medium: $\varphi_\beta = -95.3$ mV and $\Gamma^0_X = 9.1 \times 10^{16}$ sites m^{-2}. In Eqs. (19) and (20), the parameter a_i represents the activity of the species i in the

macropores, Q_0 (in C m^{-2}) is the surface charge density at the surface of the mineral, and K_i represents the speciation constant associated with the desorption of the counterion i. This model will be used to compute a prior value for K_d^{Na} of the $^{22}Na^+$ tracer in Section 5.

3.2. A model for the diffusion of tracers

Revil and Linde (2006) proposed a multi-ionic diffusion model in which flux of species i is driven by the gradient of its electrochemical potential. In the present case, there is no macroscopic electrical field because of the concentration of the tracer is much smaller than the ionic strength of the pore water. In Appendix A, we show that this model yields an apparent Fick's law Leroy et al. (2006),

$$\mathbf{J}_i = -D_i \nabla C_i, \tag{21}$$

$$D_i = \frac{\beta_i \overline{C}_i k_B T}{|q_i| C_i F}, \tag{22}$$

where D_i is the effective diffusion coefficient of the ionic species in the microporous charged medium, β_i is the corresponding ionic mobility in the bulk pore water (in m^2 s^{-1} V^{-1}), and F is the formation factor. Note that D_i is the product of three terms: (i) the self-diffusion coefficient of the ionic tracer in the water D_i^f, which is expressed by the Nernst–Einstein relation,

$$D_i^f = \frac{\beta_i k_B T}{|q_i|}, \tag{23}$$

(ii) the formation factor F which can be related to the porosity by Archie's law $F = \phi^{-m}$ (Archie, 1942), where m is called the cementation exponent with $1 \leqslant m \leqslant 3$ for most of all media (m has been determined equal to 1.95 ± 0.04 in the COx by Revil et al. (2005) and in the range 2-3 by Descostes et al., 2008), and (iii) the $\overline{C}_i/C_i$ ratio, which is given by Eq. (17).

From Eqs. (17), (22), and (23), we obtain the following relationship for the diffusivity and the effective diffusion coefficient:

$$\eta_i = \frac{D_i^f}{\phi + (1-\phi)\rho_g K_d^i} \left(\frac{1}{F}\right) \exp\left(-\frac{q_i \varphi_m}{k_B T}\right), \tag{24}$$

$$D_i = \frac{D_i^f}{F} \exp\left(-\frac{q_i \varphi_m}{k_B T}\right), \tag{25}$$

respectively. Therefore the diffusivity of an ionic tracer depends only upon three key-parameters: K_d^i, F, and φ_m. The formation factor can be obtained by a variety of methods like the measurement of the electrical conductivity of the porous material at different salinities of the brine to separate the contribution from the brine conductivity from the surface conductivity contribution (note that F is NOT the ratio of the brine conductivity to the effective conductivity of the rock as found in a number of papers). The formation factor can also be obtained by steady-state HTO (tritiated water) diffusion experiments. HTO is considered to be a non-reactive species with the mineral/water interface. Therefore the model of Revil (1999) yields $F = D_{HTO}^f / D_{HTO}$ where D_{HTO}^f is the value of self-diffusion coefficient of HTO in water and D_{HTO} represents the value of the effective diffusion coefficient of HTO through the porous material.

4. NUMERICAL SIMULATIONS AND SENSITIVITY ANALYSIS

The previous system of equations was solved by a PDE solver based on the finite-element method (the Earth Science module of COMSOL Multiphysics™ 3.4). We have checked the accuracy of the solver by comparing the results with known analytical solutions (e.g., Crank, 1970). The problem can therefore be solved in 1D, 2D, or 3D accounting for the heterogeneity in the distribution of the material properties (e.g., the formation factor) or the physicochemical parameters associated with the clay content and the clay mineralogy.

We consider below only the 1D problem of a tracer through-diffusion experiment. The through-diffusion technique is a classical laboratory method to determine the diffusion properties of consolidated clay material (e.g., Melkior et al., 2004). A small cylinder of the medium is placed between two reservoirs filled with water in chemical equilibrium with this medium. In order to study diffusion properties of a considered ionic species i, a trace concentration of a radio-active isotope is placed in the upstream reservoir. As the tracer concentration is very low, there is no real concentration gradient in the medium and therefore no electroosmotic flow and no macroscopic electrical field. Tracer concentrations in each reservoir are kept as constant as possible: trace concentration in the upstream reservoir and zero in the downstream reservoir. In general, diffusion properties of a medium are determined by tracer influx in the downstream reservoir (Melkior, 1999; Melkior et al., 2004). We use constant boundary conditions: $C_T = 10^{-14}$ mol m^{-3} (trace level) in the upstream reservoir and $C_T = 0$ mol m^{-3} in the downstream reservoir (Fig. 3). We note L (in m) the length of the core sample, which is divided into 120 elements.

We compute the evolution of the normalized ionic fluxes $\mathbf{J}_N$ (integrated over the surface area of the end-face of the core sample) in the downstream reservoir as a function of time. The flux of the ionic tracer in the downstream reservoir is normalized by the tracer concentration in the upstream reservoir and by the length L of the core sample. Thus the normalized flux $\mathbf{J}_N$ is expressed in m^2 s^{-1}. Time

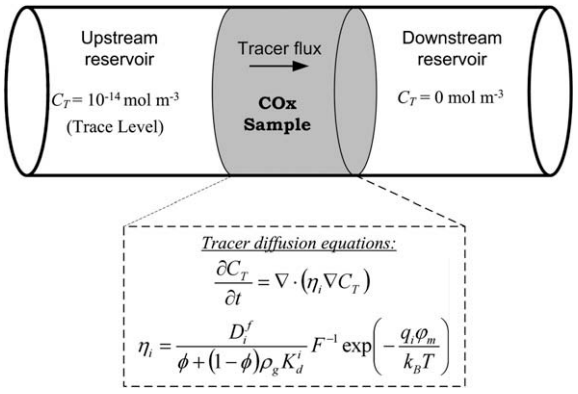

Fig. 3. Implementation sketch of our model for tracer diffusion simulation. The subscripts i and T refer for the considered ionic species and the used tracer isotope.

axis is expressed in days for convenience (the computations are all performed in SI units).

We discuss now the sensitivity of the model to its parameters described in Section 3. This synthetic case was implemented with the properties of the COx and the pore water chemistry obtained by Leroy et al. (2007). The porosity $\phi = 0.164$ yields $F = \phi^{-1.95} = 34.0$. The density $\rho_g = 2700$ kg m^{-3}, the CEC $= 0.18$ mol kg^{-1}, and the partition coefficient $f_Q = 0.94$ yield $\varphi_m = -14.9$ mV using Eqs. (13)–(16). If the partition coefficient f_Q takes the values 0.92 and 0.96, φ_m is equal to -18 and -11 mV, respectively. We consider a radio-active metal cation tracer M^+ with a total concentration (tracer and stable isotope) in the medium $C_{M^+} = 31.5 \times 10^{-3}$ mol L^{-1}, the mobility $\beta_{M^+} = 5.19 \times 10^{-8}$ m^2 s^{-1} V^{-1} and the following distribution coefficient $K_d^{M^+} = 10^{-3}$ m^3 kg^{-1}. Fig. 4 shows the sensitivity of the model to these four important parameters.

By definition (see Section 3), the formation factor F and the electrical mean potential φ_m (which depends on f_Q) influence the effective diffusion coefficient, while the distribution coefficient K_d affects only the apparent diffusion coefficient. Fig. 4a–d show the sensitivity of the model to F, φ_m, f_Q, and K_d, respectively. The model is very sensitive to these parameters. The lower the formation factor F is, the higher the diffusion flux. The parameters φ_m and f_Q are related to each other. For a cation, the lower the mean electrical potential φ_m is, the higher the normalized flux is.

5. COMPARISON WITH EXPERIMENTAL DATA

5.1. Laboratory experiments

The model presented in Section 4 is compared to tracer through-diffusion experiments in Callovo-Oxfordian clay-rock samples. We consider the following tracers (i) $^{22}Na^+$ (data from Melkior et al., 2007), (ii) $^{36}Cl^-$, and (iii) $^{35}SO_4^{2-}$ (data from Bazer-Bachi et al., 2007). The core samples used by these authors have been extracted from different locations in the COx formation. The properties of the core samples are summarized in Table 1. The samples from K100 in Bazer-Bachi et al. (2007) corresponds to a end-member of the overall formation in term of clay content and porosity (see Table 1).

Through-diffusion experiments were performed in two different core samples for $^{36}Cl^-$ and $^{35}SO_4^{2-}$. This could explain the small differences in porosities and formation factors for the two experiments. Experiments were run with a synthetic water of a composition in chemical equilibrium with the initial medium (see Table 2). Samples were put in contact with this synthetic water for several weeks to reach equilibrium. Diffusion results are presented as normalized ionic out-flux J_N measured in the downstream reservoir versus time. This allows the comparison between results for different values of the thickness and the diameter of the samples.

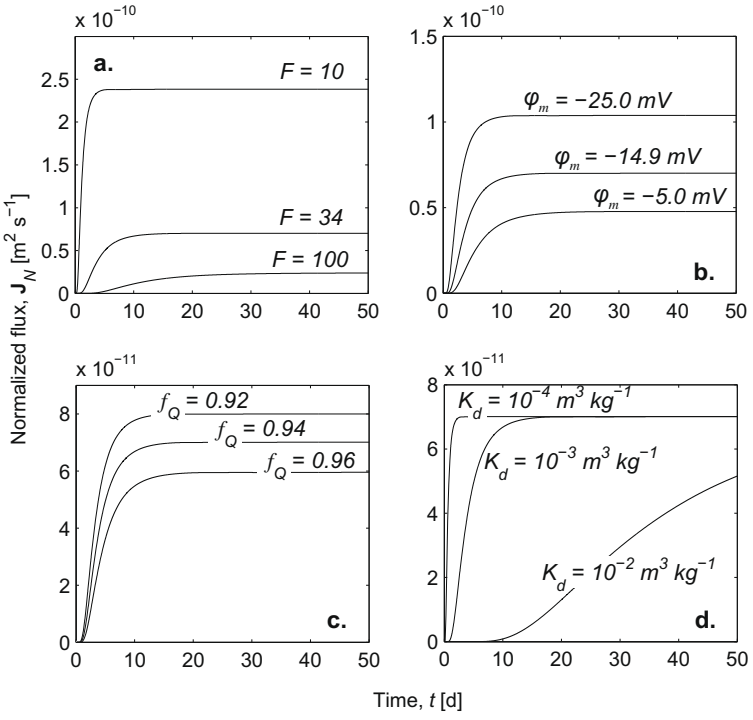

Fig. 4. Model sensitivity of four important parameters on the normalized diffusion flux $\mathbf{J}_N$ expressed as a function of time (in days, d): (a) influence of the formation factor F, (b) influence of the mean electrical potential φ_m in the microporosity (c) Influence of the partition coefficient f_Q of the countercharge between the Stern and the diffuse layers, and (d) Influence of the distribution coefficient K_d. Note that in the steady-state regime, the normalized flux is independent of the value of K_d. The value of K_d influences the characteristic time of the transient period but not the steady state value of the flux.

Table 1
Physical and chemical characteristics of the through-diffusion samples.

	HTM102 (−464 m)	EST205-K100
Porosity, ϕ	0.15	0.030–0.037[a]
Grain density, ρ_g (kg m^{-3})	2670	2700[b]
Cation exchange capacity CEC (meq g^{-1})	0.18 ± 0.04[c]	0.11 ± 0.03[d]
Temperature, T (K)	296 (23 °C)	294 (21 °C)
Depth (m)	464	424
Lithofacies	C2b2	C2d

[a] HTO apparent porosity for tracer $^{36}Cl^-/^{35}SO_4^{2-}$ disk, respectively.
[b] Leroy et al. (2007).
[c] Gaucher et al. (2004) and Leroy et al. (2007).
[d] ANDRA (2005).

Table 2
Ionic compositions of the synthetic ground water.

	Concentration (mol L^{-1})	
	Melkior et al., 2007	Bazer-Bachi et al., 2007[a]
Na^+	3.44×10^{-2}	4.17×10^{-2}
K^+	1.34×10^{-4}	5.40×10^{-3}
Ca^{2+}	2.87×10^{-3}	9.74×10^{-3}
Mg^{2+}	5.26×10^{-3}	7.68×10^{-3}
Cl^-	5.00×10^{-2}	7.19×10^{-2}
SO_4^{2-}	7.00×10^{-5}	4.40×10^{-3}
HCO^{3-}	6.20×10^{-4}	1.44×10^{-3}
I[b]	5.70×10^{-2}	1.03×10^{-1}
pH	8.0	7.3

[a] From Jacquot (2002).
[b] Ionic strength.

In order to compare the model with the experimental data, we first determine prior values for the three key-parameters (the formation factor, the mean electrical potential of the pore space, and the sorption coefficients). For each sample, HTO diffusion data are used to determine the prior value of the formation factor using $F = D_{HTO}^f / D_{HTO}$. Results are given in Table 3. Then, from the synthetic porewater composition and the model described in Section 3.1, we determine the a priori, value of the mean electrical potential φ_m (see Eqs. (13)–(16)). They are given in Table 3 using the value $f_Q = 0.94$ discussed above. We use the distribution coefficients K_d^i given by Melkior et al. (2007) for his sample. This distribution coefficient has been determined by batch test experiments. The prior values of the distribution coefficient of cations (counterions) can also be obtained from Eqs. (18)–(20). Therefore, we will compare this result for $^{22}Na^+$ in the sample HTM102 (−464 m deep) to the K_d value obtained by batch experiment from Melkior et al. (2007).

For each data set, we fit the data with the Simplex algorithm (Caceci and Cacheris, 1984) to obtain the posterior values of the key-parameters F, φ_m, and K_d^i. The forward problem, solved by COMSOL Multiphysics™ 3.4, is coupled to an optimization routine written in a MatLab® routine (Fig. 5). Our algorithm looks for the minimum of a cost function G define by,

$$\mathrm{Min}G \equiv \sum_{i=1}^{N} \left| \frac{\mathbf{J}^i_{\mathbf{N}Exp} - \mathbf{J}^i_{\mathbf{N}Model}}{\mathbf{J}^i_{\mathbf{N}Model}} \right| + \frac{2}{3} R, \tag{26}$$

$$R \equiv \left| \frac{F^{opt} - F^{ap}}{F^{ap}} \right| + \left| \frac{\varphi_m^{opt} - \varphi_m^{ap}}{\varphi_m^{ap}} \right| + \left| \frac{K_d^{opt} - K_d^{ap}}{K_d^{ap}} \right|, \tag{27}$$

where N is the number of the experimental data i, and R a regularization term (see Tikhonov, 1963). The superscripts "opt" and "ap" mean optimized and prior parameters, respectively. Fig. 6 shows that the cost function G has an unique minimum.

Fig. 7 presents fitted formation factors of the investigated samples versus the porosity. We also plotted F from bibliographic data on the Callovo-Oxfordian and Archie's law $F = \phi^{-m}$ (for $m = 1.95$ and $m = 3$) on this figure to show the consistency of the fitted values. We note that $m = 3$ correspond to the proposed value of Mendelson and Cohen (1982) for platey disks (like montmorillonite). Note that these formation factors results also from different evaluations: Revil et al. (2005) obtained their formation factors (Fig. 7a) from electrical conductivity measurement at different salinities while the values proposed by Descostes et al. (2008) are based on HTO diffusion data (Fig. 7b).

Fig. 8 shows the fitted mean electrical potential versus porosity compared to the model of Revil and Linde (2006) described in Eqs. (13)–(16), using the porewater chemistry given by the bibliography (Table 2).

The apparent distribution coefficient $K_d^{Na^+}$ studied by Melkior et al. (2007) can be calculated following our ap-

Table 3
Computed a priori parameters for tracer diffusion simulation.

	Tracer	Porosity, ϕ	Formation factor, F	Electrical mean potential, φ_m (V)	Distribution coefficient, K_d (m^3 kg^{-1})
HTM102 (−464 m)	$^{22}Na^+$	0.150	89.6	-23.2×10^{-3}	0.41×10^{-3}[a]
EST205-K100	$^{36}Cl^-$	0.030[b]	772.3	-32.1×10^{-3}	0
	$^{35}SO_4^{2-}$	0.037[b]	717.1	-29.1×10^{-3}	0[c]
					0.018×10^{-3}[d]

[a] Measured by batch experiment by Melkior et al. (2007).
[b] Apparent porosity from HTO diffusion.
[c] Result from batch experiment by Bazer-Bachi et al. (2007).
[d] Measured by column experiment by Bazer-Bachi et al. (2007).

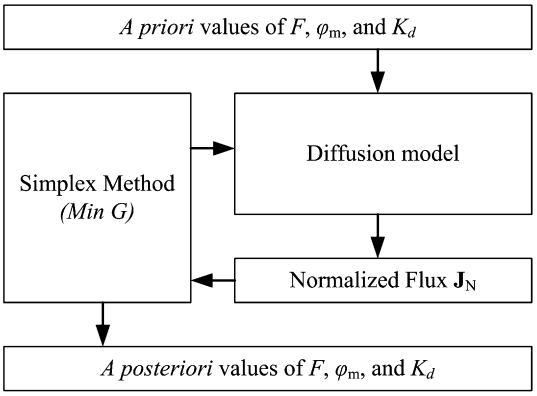

Fig. 5. Optimization algorithm for model parameters determination from experimental normalized flux. The COMSOL Multiphysics™ program provides the normalized diffusion flux data and the Simplex algorithm minimize a cost function G to fit these data, and then determine the best value of the formation factor, the mean electrical potential in the microporosity, and the partition coefficient for sorption.

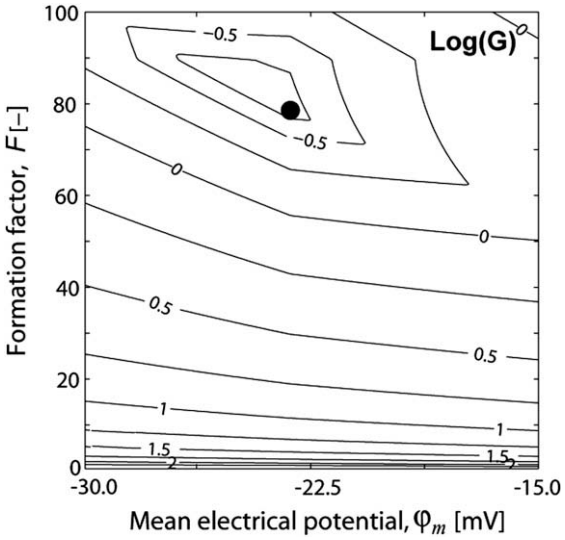

Fig. 6. Shape of the logarithm of the cost function with a regularization term for the optimization of the $^{22}Na^{+}$ diffusion experiment (HTM102 −464 m). The cost function G has a unique minimum corresponding to the position of the filled circle.

proach based on the triple layer model (using Eqs. (18)–(20)) and used as an a priori parameter. This computation used COx parameters: $\varphi_\beta = -95.3 \times 10^{-3}$ V, $\Gamma^0_X = 9.1 \times 10^{16}$ sites m^{-2} (from Leroy et al., 2007), and $S_{sp} = 5 \times 10^4$ m^2 kg^{-1} (from Gaucher et al., 2004). Leroy et al. (2007) have also determined $K_{Na} = 0.80 \pm 0.05$, which is consistent with the value proposed by Avena and De Pauli (1998) ($K_{Na} = 0.77$). Using the pore water composition proposed by Melkior et al. (2007) ($C_{Na^+} = 3.44 \times 10^{-3}$ mol L^{-1}), Eq. (19) yields the surface site density of counterions in the Stern layer equal to $\Gamma^0_{XNa} = 1.72 \times 10^{17}$ sites m^{-2}.

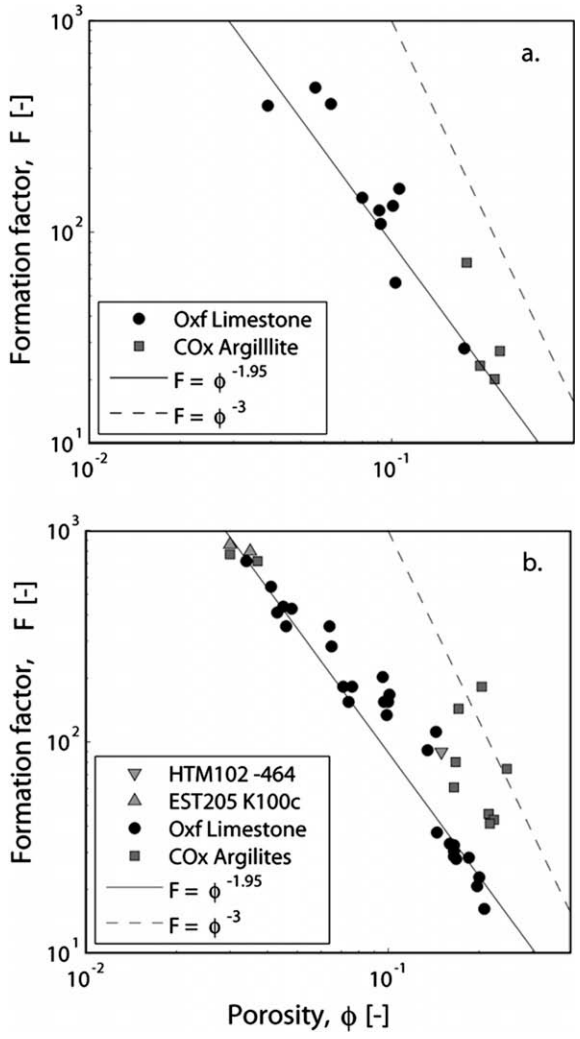

Fig. 7. Formation factor versus porosity in the COx argillite. The formation factor data have been obtained: (a) by electrical measurement for Revil et al. (2005), (b) by the ratio $F = D^f_{HTO}/D_{HTO}$ for Descostes et al. (2008), and by fit for HTM102-464 and EST205-K100 in the present study (a posteriori value). Archie's law for $m = 1.95$ and $m = 3$ have been proposed by Revil et al. (2005) and Descostes et al. (2008), respectively, (Oxf stands for Oxfordian).

5.1.1. Diffusion of $^{22}Na^{+}$

We ran an optimization procedure for the $^{22}Na^{+}$ tracer diffusion data for sample HTM102 (464 m deep) (Melkior et al., 2007). The value of the distribution coefficient they found by a batch experiment is equal to 0.41×10^{-3} m^3 kg^{-1}. Using the TLM model of Leroy et al. (2007), we determine a prior value of $K_d = 0.414 \times 10^{-3}$ m^3 kg^{-1} which corresponds to an excellent agreement between the TLM model and the experimental value by a batch experiment. Prior values for the formation factor and the mean electrical potential are $F = 89.6$ and $\varphi_m = -23.2$ mV, respectively.

The fitted normalized flux curve and experimental data are presented in Fig. 9. The best fit yields the following posterior values: $F = 82.6$, $\varphi_m = -23.8$ mV, and $K_d = 0.704 \times 10^{-3}$ m^3 kg^{-1} (the correlation coefficient is

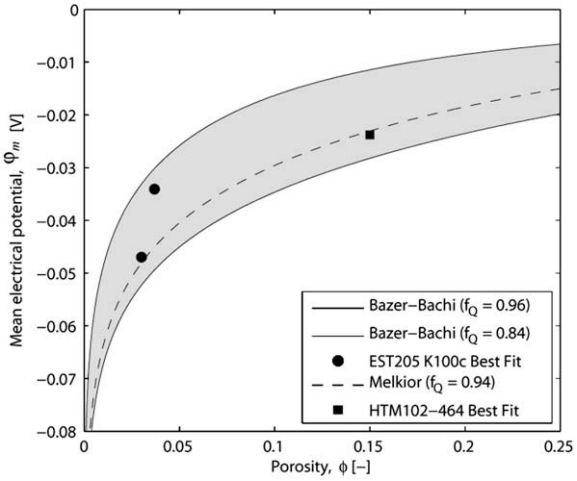

Fig. 8. Fitted mean electrical potential for the three samples and model prediction versus porosity. The mean electrical potentials are determined from the water chemistry used by Bazer-Bachi et al. (2007) for the diffusion experiments (solids lines), and by Melkior et al. (2007) (dashed line). The gray envelop corresponds to two values of the Stern fraction of counterion: the maximum value proposed by Leroy et al. (2007) ($f_Q = 0.96$), and the lower calculated value resulting from the osmotic pressure data ($f_Q = 0.84$). The filled circles and square represent the best fit from the experimental data of Bazer-Bachi et al. (2007) and Melkior et al. (2007), respectively.

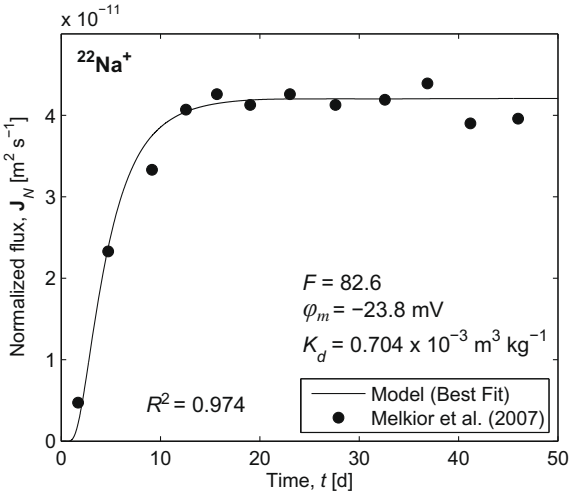

Fig. 9. Simulation of a $^{22}Na^+$ tracer diffusion in the COx (HTM102 −464 m deep).

$R^2 = 97.4\%$). The fitted and the computed formation factor F are very close ($RE = 7.9\%$). The mean electrical potential fitted corresponds pretty well to the computed one ($RE = 2.6\%$). The distribution coefficient presents a difference ($RE = 41.8\%$). This difference between fitted and computed parameters can easily be explained by the uncertainties both on the experimental data, on the porosity, and on the value of F resulting from HTO diffusion data.

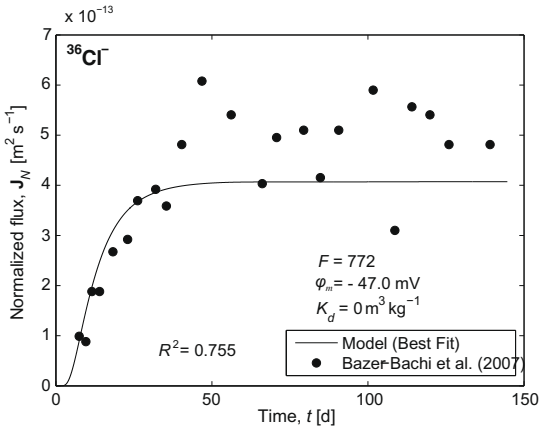

Fig. 10. Simulation of a $^{36}Cl^-$ tracer diffusion in the COx (EST205-K100).

5.1.2. Diffusion of $^{36}Cl^-$

We ran the simulation for $^{36}Cl^-$ tracer diffusion in the EST205-K100. Fig. 10 shows the confrontation between the fitted normalized diffusion flux following our model and experimental data from Bazer-Bachi et al. (2007). The chloride $^{36}Cl^-$ is a non-sorbed tracer, so we consider $K_d = 0$ m^3 kg^{-1}. The other a priori value are $F = 772.3$ and $\varphi_m = -32.1$ mV.

The minimization of the cost function G yields the following a posterior values of the model parameters: $F = 772.3$ and $\varphi_m = -47.0$ mV ($R^2 = 75.5\%$). Computed and fitted formation factor F are equal but the a posteriori value of mean electrical potential φ_m presents a difference with the a priori value ($RE = 46.9\%$).

5.1.3. Diffusion of $^{35}SO_4^{2-}$

We have also simulated the $^{35}SO_4^{2-}$ diffusion data through a clay-rock sample from the EST205-K100 core (Bazer-Bachi et al., 2007). Concerning the sulfate tracer, we took into account ion pairing. Indeed, sulfate speciation reactions have quite hight reaction coefficient and the complexes resulting from these reactions have diffusion coefficient on the same order of magnitude than SO_4^{2-} (see Table 4). Some of the sulfate species are uncharged ($CaSO_4^0$ and $MgSO_4^0$). This means that their diffusion coefficient depends only on the formation factor F and not on the electrostatic tortuosity δ_{el}. Bazer-Bachi et al. (2007) used radio-active measurement (normalized flux in [(Bq m^{-2} d^{-1})/(Bq m^{-3})]) in the downstream reservoir, which means that every radio-active $^{35}SO_4$species were measured (not only $^{35}SO_4^{2-}$). Thus the measured flux of $^{35}SO_4$ is the sum of all the $^{35}SO_4$ species flux: $\mathbf{J}_{SO_4} = \sum p_j \mathbf{J}_j$, where p_j is the concentration fraction of the considered SO_4 species. We used the software PHREEQC (version 2) developed by Parkhurst and Appelo (1999) to compute the speciation using the Bazer-Bachi et al. (2007) water composition. Table 5 summarizes the major species concentrations. The tracer diffusion model is then modified to compute the following SO_4 total flux:

$$\mathbf{J}_{SO_4} = p_{SO_4^{2-}} \mathbf{J}_{SO_4^{2-}} + p_{NaSO_4^-} \mathbf{J}_{NaSO_4^-} + p_{KSO_4^-} \mathbf{J}_{KSO_4^-} + p_{CaSO_4^0} \mathbf{J}_{CaSO_4^0} + p_{MgSO_4^0} \mathbf{J}_{MgSO_4^0}. \quad (28)$$

Table 4
Reactions and constants for the speciation of sulfate (at 25 °C).

Chemical reaction	Speciation constant[a]	Diffusion coefficient ($m^2\ s^{-1}$)[a]
$Ca^{2+} + SO_4^{2-} \leftrightarrow CaSO_4^0$	$K_{Ca} = 2.3$	$D^f_{CaSO_4^0} = 5.06 \times 10^{-10}$
$Mg^{2+} + SO_4^{2-} \leftrightarrow MgSO_4^0$	$K_{Mg} = 2.34$	$D^f_{MgSO_4^0} = 4.78 \times 10^{-10}$
$K^+ + SO_4^{2-} \leftrightarrow KSO_4^-$	$K_K = 0.85$	$D^f_{KSO_4^-} = 7.16 \times 10^{-10}$
$Na^+ + SO_4^{2-} \leftrightarrow NaSO_4^-$	$K_{Na} = 0.7$	$D^f_{NaSO_4^0} = 6.18 \times 10^{-10}$

[a] Value proposed by the PhreeqC2 manual by Parkhurst and Appelo (1999).

Table 5
Major species of the Bazer-Bachi et al. (2007) solution calculated from Table 2 and PHREEQC2.

Major ionic species	Concentration ($mol\ L^{-1}$)	Species fraction of $[SO_4^{tot}]$[a]
Na^+	4.19×10^{-2}	
$NaSO_4^-$	8.91×10^{-5}	0.04
K^+	5.42×10^{-2}	
KSO_4^-	1.50×10^{-4}	0.07
Ca^{2+}	9.38×10^{-3}	
$CaSO_4^0$	2.85×10^{-4}	0.14
Mg^{2+}	7.28×10^{-3}	
$MgSO_4^0$	2.54×10^{-4}	0.13
Cl^-	7.24×10^{-2}	
SO_4^{2-}	1.23×10^{-3}	0.61
HCO_3^-	6.79×10^{-4}	

[a] $p_i = \frac{C_i}{\sum[SO_4]}$.

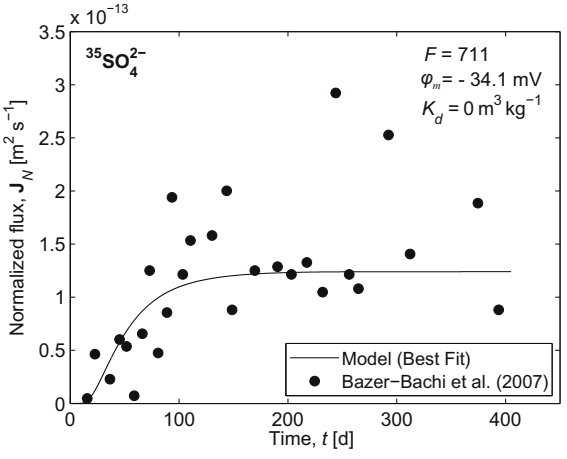

Fig. 11. Simulation of a $^{35}SO_4^{2-}$ tracer diffusion in the COx (EST205-K100).

Bazer-Bachi et al. (2007) performed two different tests on COx argillites to determine the SO_4 sorption: a column test led to $K_d = 1.80 \times 10^{-5}\ m^3\ kg^{-1}$, but the batch experiment did not show sorption. The prior values of formation factor and mean electrical potential are $F = 717.1$, $\varphi_m = -29.1$ mV, and $K_d = 0\ m^3\ kg^{-1}$, respectively.

The minimization of the cost function G yields the following posterior values: $F = 711$ and $\varphi_m = -34.1$ mV ($R^2 = 46.7\%$) in good agreement with the experimental value given above (Fig. 11). The strong dispersion of the experimental data yields a low R^2 fit value. However, the fitted and computed formation factors F are very close to each other ($RE = 0.8\%$). The fitted mean electrical potential φ_m present a bigger difference ($RE = 14.7\%$). The difference between the two fitted φ_m can be explained by the model sensitivity and experimental uncertainty.

6. FIELD DATA

In a recent study, Descostes et al. (2008) determined the diffusion coefficients of several anions (Cl^-, I^-, SO_4^{2-}, and SeO_3^-) in a set of the Callovo-Oxfordian clay-rock samples formation and in the Oxfordian limestones, which is the formation lying just above the COx formation in the Paris Basin. From the top of the Oxfordian formation to 399 m deep, the formation is composed of several calcareous facies (called C3b, L1a, L1b, L2a, L2b, and L2c) with 80–95% of carbonates (ANDRA, 2005). Between 399 and 417 m deep, the Oxfordian formation presents important vertical mineralogical variations (facies C3a). The carbonate fraction decreases roughly from 80% (at a depth of 399 m) to less than 40% (at a depth of 417 m) while the clay fraction increases from 15% to 45% (illite, mica, and interstratified illite/smectite). The remaining mineral corresponds mainly to silica. The upper part of the COx formation (facies C2d, 417–437 m deep) presents important spatial variations in the mineralogy. These variations are in the same order of magnitude than in C3a. Below 437 m, the COx becomes more homogeneous with a fraction of 40–50% of clay minerals, 20–35% of carbonates, and 25–35% of silica (facies C2b1, C2b2, and C2c) (ANDRA, 2005).

The measurements of the diffusion coefficients were performed with the through-diffusion technique using a collection of core samples from 166 m to 477 m below the ground surface. For each sample for which the anionic diffusion was made, except for SeO_3^-, the HTO diffusion coefficient was also measured. We did not consider the I^- tracer diffusion experiments because the iodine is not present in the natural COx clay-rock. Concerning sulfate, we considered the speciation model of ion pairing discussed above (Section 5.1.3., and Tables 4 and 5) for the φ_m calculation. We used first the HTO diffusion coefficients to determine the values of the formation factor using $F = D^f_{HTO}/D_{HTO}$ (see Fig. 7b). Then, using Eq. (25), we determined the mean electrical potential φ_m from F and D_i (in the range (0.2–96) $\times 10^{-12}\ m^2\ s^{-1}$):

$$\varphi_m = -\frac{k_B T}{q_i} \log\left(\frac{D_i F}{D_i^f}\right). \tag{29}$$

Fig. 12 shows the values of F and φ_m as a function of depth. The calculated formation factor in the upper part of the Oxfordian limestone formation (from 177 to 360 m deep) is quite low. It becomes more important and reach 10^3 between 400 and 425 m just above the Callovo-Oxfordian argillites. The C3a layer has been particularly studied by Descostes et al. (2008) with six samples between 399 and 417 m deep. In the middle of the COx formation, F is

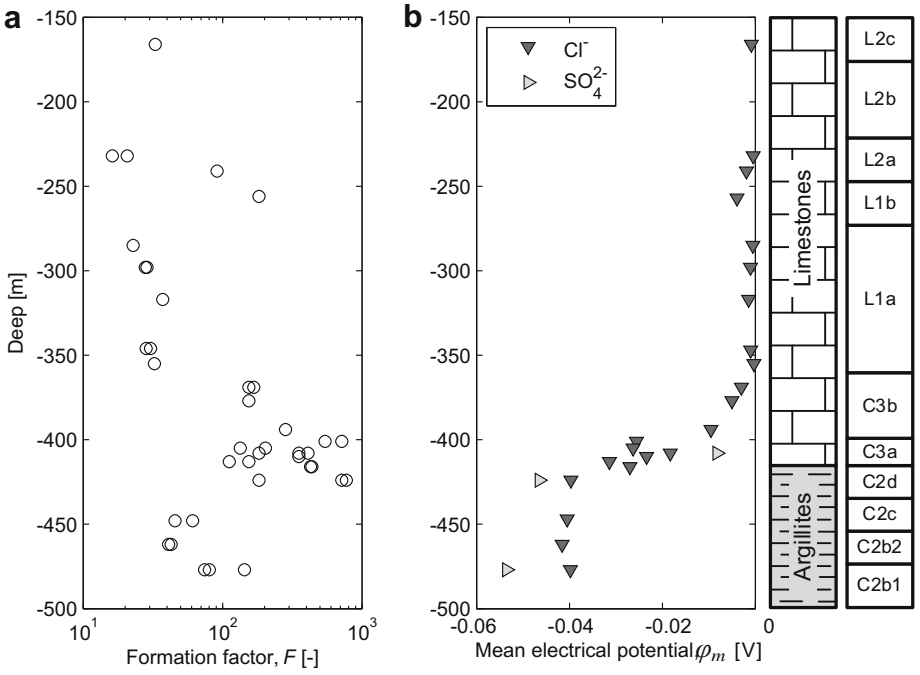

Fig. 12. Computation of F (a) and φ_m (b) in the Paris basin as a function of depth using the experimental data from Descostes et al. (2008). Samples were collected in the well EST-205. This borehole crosses the formation of Oxfordian limestones (160–417 m below ground level) and the Callovo-Oxfordian clay-rock (417–550 m).

comprised between 40 and 140, which is consistent with the electrical conductivity measurements presented by Revil et al. (2005) and performed at different salinities with NaCl brines.

The values of φ_m are very low in the Oxfordian limestone formation. In this formation, we have,

$$\lim_{\varphi_m \to 0} D_i/D_i^f = 1/F, \tag{30}$$

which means that the electrostatic constrictivity δ_{el} is equal to one. The C3a layer (399–417 m deep) presents more important values of the mean potential in the microporosity φ_m. The values of φ_m are in the range between -40 and -20 mV.

In the COx formation, the mean electrical potential that is calculated falls between -54 and -39 mV. Considering the experimental uncertainties and the local variation of parameters (ϕ, CEC) between two samples, the computed φ_m are quite consistent with the average of computed electrical potential: -43.5 mV in the COx. This electrical potential value appears to be stronger than the model predictions by Eqs. (13)–(16).

Our tracer diffusion model is directly related to the generalized transport model in microporous media described by Revil and Linde (2006). That implies that parameters like the electrical formation factor F and the mean electrical potential in the diffuse layer φ_m, can be applied to determine some other rock properties. The osmotic pressure is one of them. Therefore, in order to test further the range of computed φ_m values, we decided to compute the value of the osmotic pressure in the COx from the diffusion test data. Revil and Linde (2006) proposed the following relationship between the mean electrical potential φ_m and the osmotic pressures π_m:

$$\pi_m = k_B T \sum_{i=1}^{Q} C_i \left[\exp\left(-\frac{q_i \varphi_m}{k_B T} \right) - 1 \right], \tag{31}$$

where Q is the number of species that are present in the pore water solution. The osmotic efficiency is defined by,

$$\varepsilon \equiv \left(\frac{\partial p}{\partial \pi_m} \right)_{u=0}, \tag{32}$$

and $\varepsilon \leqslant 1$ ($\varepsilon = 1$ for a perfect membrane). Therefore in an undrained system (the Darcy velocity $\mathbf{u}$ is zero), the fluid pressure is equal to $p = p_H + \varepsilon \pi_m$. Therefore the excess fluid pressure is equal to,

$$\delta p \equiv p - p_H = \varepsilon \pi_m. \tag{33}$$

where the hydrostatic fluid pressure is taken in the underlying Dogger limestones formation.

Considering the pore water presented in Descostes et al. (2008), it becomes possible to determine π_m in the COx at several depths from the previously determined values of φ_m (using Eq. (29)). The values of the osmotic pressure are shown on Fig. 13. The predicted values can be compared to the measured fluid overpressure (above the hydrostatic level) in the Callovo-Oxfordian argillites layer (see Gueutin et al., 2007). The measured excess hydraulic heads are in the range 20–60 m (0.2–0.6 MPa). Comparison between measured overpressure and computed osmotic pressure π_m in the medium are displayed on Fig. 13. The computed values of φ_m from Cl^- and SO_4^{2-} diffusion tests (Descostes et al., 2008) are used to determine the osmotic pressure in the COx Formation. Using Eq. (33) and the measured overpressures, this yields a value for the osmotic efficiency $\varepsilon \approx 0.4$.

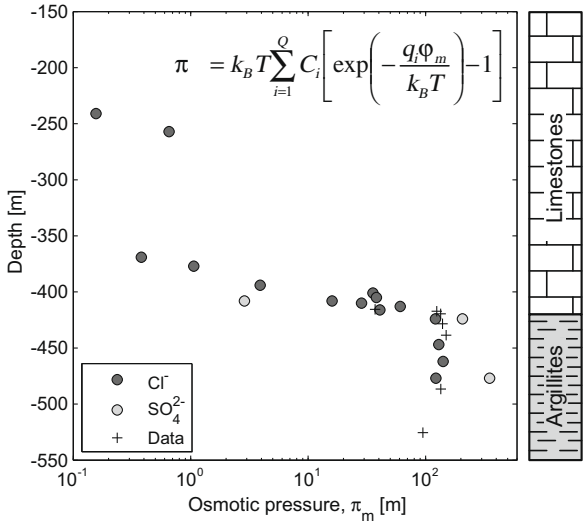

Fig. 13. Comparison between the osmotic head π_m in the Oxfordian Limestones and Callovo-Oxfordian argillites and the measurements of the excess pore fluid pressure head (above hydrostatic) with $\varepsilon = 0.40$ (Eq. (33)).The values of π_m have been determined from the values of φ_m (Fig. 13) and synthetic pore water described in Descostes et al. (2008). The overpressure data (+) (here expressed in hydraulic head above hydrostatic) come from ANDRA (Gueutin et al., 2007).

Can the previous value of the osmotic coefficient value be determined independently? The response is yes. Indeed, Revil and Leroy (2004) and Revil et al. (2005) developed a model for the osmotic coefficient that is given by,

$$\varepsilon = 1 - (1 + R^2)^{1/2} + R(2\, T_{(+)} - 1), \tag{34}$$

where $T_{(+)}$ is the macroscopic Hittorf number of the cations through the clay-rock and R is an adimensional number defined by $R = \overline{Q}_V/(2eC_f)$ for a binary symmetric electrolyte. Eq. (34) was tested successfully against experiment data by Revil and Leroy (2004). Determining the value of $\overline{Q}_V$ from Eqs. (13) and (14) and using $f_Q = 0.84$, yields $T_{(+)} = 0.9$ and $R = 1.77$. In turn, plugging these values into Eq. (34) yields $\varepsilon = 0.40$. This value agrees with the value determined above from the excess head pressure recorded in the borehole (Fig. 13). Taking into account all the uncertainties yields ε comprised between 0.20 and 0.40. These values correspond to f_Q in the range 0.84 to 0.90. This upper value of f_Q is close to the one proposed by Leroy et al. (2007) and the lower value corresponds to Gonçalvès et al. (2007) value for a bentonite.

How the osmotic pressure is responsible for an observed overpressure? The osmotic swelling pressure is responsible for the swelling of the walls of the borehole drilled through the COx formation. The good agreement between the trend of the computed osmotic swelling pressure and that of the fluid overpressure measured in boreholes could be interpreted as the result of a related swelling of the clay-rock. This swelling yields a constriction of the walls of the well and thus a reduction of the volume of the chamber where the pressure probe is measuring the pressure.

7. CONCLUSION

The model developed by Revil and Linde (2006) is used to compute the diffusion of tracers ($^{22}Na^+$, $^{36}Cl^-$, $^{35}SO_4{}^{2-}$) through the Callovo-Oxfordian clay-rock using a generalized Donnan equilibrium model and the formation factor. This model is able to explain tracer diffusion experiments performed by different authors in the COx formation and to determine the profile of these parameters in the formations. In addition, the mean electrical potential allows the determination of the osmotic pressure in the medium. The next step will be to connect this diffusion model to geophysical measurements of complex resistivity such as modeled recently by Leroy et al. (2008) to evaluate the properties of the excavation damaged zone in the vicinity of the galleries of an underground site. In fact, the model developed in the present paper is also easy to extend to unsaturated conditions. Revil and Jougnot (2008) have discussed recently a model of multicomponent diffusion in an unsaturated porous material. The change of variables $1/F \rightarrow \phi^m s_w^n$ and $\overline{Q}_V \rightarrow \overline{Q}_V/s_w$ (where s_w is the relative water saturation) provides a theoretically justified operation to determine the effect of the water saturation upon the effective diffusion coefficient of ionic tracers in a clay-rock.

ACKNOWLEDGMENTS

We thank the French National Research Council (CNRS) and the French National Agency for Radioactive Waste Management (ANDRA) (S. Altmann and D. Coelho) for their support. J. Lancelot is thanked for his support through the GDR FORPRO. The Ph.D. thesis of Damien Jougnot is supported by ANDRA. A. Revil strongly thanks T. Young for his support at CSM. D. Jougnot thanks A. Jardani and J.C. Robinet. We thank C.A.J. Appelo and two anonymous referees for their very constructive reviews of this manuscript.

APPENDIX A

In this Appendix, we estimate the influence of the activity coefficient upon the diffusion of the tracers through a clay-rock. From Revil and Linde (2006), the constitutive equation of the diffusion flux of a single ion is writen as:

$$\mathbf{J}_i = -\frac{\bar{\sigma}_i}{q_i^2 F} \nabla \mu_i, \tag{A1}$$

with F, the formation factor, $q_i = (\pm e) z_i$, the charge of species i and z_i its valence ($e = 1.6 \times 10^{-19}$ C is the elementary charge), and $\bar{\sigma}_i = \beta_i \overline{C}_i |q_i|$ the contribution of species i to the overall electrical conductivity of the pore water (in S m^{-1}) defined from β_i the ionic mobility and $\overline{C}_i$ the concentration of species i in the pore space. The chemical potential μ_i is related to the ionic activity a_i by $\mu_i = \mu_i^0 + k_B T \ln a_i$ where μ_i^0 is the reference chemical potential. This yields,

$$\mathbf{J}_i = -\frac{k_B T \beta_i \overline{C}_i}{|q_i| F} \nabla \ln a_i. \tag{A2}$$

The first Fick's law defines the ionic flux as a function of the concentration gradient. The relationship between the

activity and the concentration is $a_i = \gamma_i C_i$ where γ_i is the activity coefficient. This yields,

$$\nabla \ln a_i = \frac{\nabla(\gamma_i C_i)}{\gamma_i C_i} = \frac{\nabla C_i}{C_i}\left(1 + \frac{C_i}{\gamma_i}\frac{d\gamma_i}{dC_i}\right). \quad \text{(A3)}$$

From (A1)–(A3), we obtain,

$$\mathbf{J}_i = -\frac{k_B T \beta_i \overline{C}_i}{|q_i| F C_i}(1 + \Theta)\nabla C_i, \quad \text{(A4)}$$

$$\Theta \equiv \frac{C_i}{\gamma_i}\frac{d\gamma_i}{dC_i} = C_i \frac{d \ln \gamma_i}{dC_i}, \quad \text{(A5)}$$

where Θ is a correction term. For a ionic strength I lower than $0.5\ \text{mol L}^{-1}$, γ_i can be computed by the Davies equation:

$$\log_{10}\gamma_i = -\frac{1}{2} z_i^2 \left(\frac{\sqrt{I}}{1+\sqrt{I}} - 0.3I\right). \quad \text{(A6)}$$

This yields,

$$\Theta = -\frac{\ln 10}{2} z_i^2 C_i \left[\frac{d}{dI}\left(\frac{\sqrt{I}}{1+\sqrt{I}}\right) - 0.3\right]\frac{dI}{dC_i}, \quad \text{(A7)}$$

$$\Theta = -\frac{\ln 10}{2} z_i^2 C_i \left[\frac{1}{2\sqrt{I}\left(1+\sqrt{I}\right)^2} - 0.3\right]\frac{dI}{dC_i}. \quad \text{(A8)}$$

From the definition of the ionic strength,

$$I \equiv \frac{1}{2}\sum_{k=1}^{Q} z_k^2 C_k, \quad \text{(A9)}$$

$$\frac{dI}{dC_i} = \frac{1}{2} z_i^2. \quad \text{(A10)}$$

The correction parameter becomes:

$$\Theta = -\frac{\ln 10}{4} z_i^4 C_i \left[\frac{1}{2\sqrt{I}\left(1+\sqrt{I}\right)^2} - 0.3\right]. \quad \text{(A11)}$$

The correction term $(1 + \Theta)$ in Eq. (A4) is always negligible $\Theta \ll 1$ when the ionic strength is close to $0.1\ \text{mol L}^{-1}$ and bigger. Neglecting the term Θ, Eq. (A3) yields an apparent Fick's law,

$$\mathbf{J}_i = -\frac{\beta_i \overline{C}_i k_B T}{|q_i| C_i F}\nabla C_i. \quad \text{(A12)}$$

REFERENCES

ANDRA (2005) Dossier 2005 argile—Référentiel du site Meuse/Haute-Marne, International Report ANDRA No. C.RP.ADS.04.0022.

Appelo C. A. J. and Wersin P. (2007) Multicomponent diffusion modeling in clay systems with application to the diffusion of tritium, iodide, and sodium in opalinus clay. *Environ. Sci. Technol.* **41**, 5002–5007.

Appelo C. A. J., Vinsot A., Mettler S. and Wechner S. (2008) Obtaining the porewater composition of a clay-rock by modeling the in- and out-diffusion of anions and cations from an in-situ experiment. *J. Contam. Hydrol.* **101**, 67–76.

Archie G. E. (1942) The electrical resistivity log as an aid in determining some reservoir characteristics. *Trans. AIME* **146**, 54–62.

Avena M. J. and De Pauli C. P. (1998) Proton adsorption and electrokinetics of an Argentinean montmorillonite. *J. Colloid Interface Sci.* **202**, 195–204.

Bazer-Bachi F., Tevissen E., Descostes M., Grenut B., Meier P., Simonnot M.-O. and Sardin M. (2005) Characterization of iodide retention on Callovo-Oxfordian argillites and its influence on iodide migration. *Phys. Chem. Earth* **31**, 517–522.

Bazer-Bachi F., Descostes M., Tevissen E., Meier P., Grenut B., Simonnot M.-O. and Sardin M. (2007) Characterization of sulphate sorption on Callovo-Oxfordian argillites by batch, column and through-diffusion experiments. *Phys. Chem. Earth* **32**, 552–558.

Bernabé Y. and Revil A. (1995) Pore-scale heterogeneity, energy dissipation and the transport properties of rocks. *Geophys. Res. Lett.* **22**(12), 1529–1552.

Bourg I. C., Bourg A. C. M. and Sposito G. (2003) Modeling diffusion and adsorption in compacted bentonite: a critical review. *J. Contam. Hydrol.* **61**, 293–302.

Bourg I. C. (2004) Caractérisation du comportement d'une bentonite sodique pour l'isolement des déchets: transport diffusif des traceurs ioniques (Na^+, Sr^{2+}, Cs^+ et Cl^-) dans la bentonite sodique compactée saturée, et titration acide-base de la montmorillonite. Ph.D. thesis, Université de Pau et des Pays d'Adour, Pau.

Bourg I. C., Sposito G. and Bourg A. C. M. (2006) Tracer diffusion in compacted, water-saturated bentonite. *Clays Clay Miner.* **54**, 363–374.

Caceci M. and Cacheris W. P. (1984) Fitting curves to data. The simplex algorithm is the answer. *Byte* **9**, 340–362.

Cey B. D., Barbour S. L. and Hendry M. J. (2001) Osmotic flow through a Cretaceous clay in southern Saskatchewan, Canada. *Can. Geotech. J.* **38**(5), 1025–1033.

Chatterji S. (2004) Ionic diffusion through thick matrices of charged particles. *J. Colloid Interface Sci.* **269**, 186–191.

Crank J. (1970) *The Mathematics of Diffusion*. Clerendon Press, Oxford.

Descostes M., Blin V., Bazer-Bachi F., Meier P., Grenut B., Radwan J., Schlegel M. L., Buschaert S., Coelho D. and Tevissen E. (2008) Diffusion of anionic species in Callovo-Oxfordian argillites and Oxfordian limestones (Meuse/Haute-Marne, France). *Appl. Geochem.* **23**, 655–677.

Eriksen T. E., Jansson M. and Molera M. (1999) Sorption effects on cation diffusion in compacted bentonite. *Eng. Geol.* **54**, 231–236.

Escoffier S., Homand F. and Giraud A. (2000) Perméabilité et coefficient de Biot des argilites de MHM. In *Recherches pour le Stockage des Déchets Radioactifs à Haute Activité et à Vie Longue, Bilan des Etudes et Travaux 2000* (eds. The French Nuclear Waste Agency) pp. 206–216.

Gasc-Barbier M., Chanchole S. and Bérest P. (2004) Creep behavior of Bure clayey rock. *Appl. Clay Sci.* **26**, 449–458.

Gaucher E., Robelin C., Matray J. M., Negrel G., Gros Y., Heitz J. F., Vinsot A., Rebours H., Cassabagnere A. and Bouchet A. (2004) ANDRA underground research laboratory: interpretation of the mineralogical and geochemical data acquired in the Callovo-Oxfordian Formation by investigative drilling. *Phys. Chem. Earth* **29**, 55–77.

Gaucher E., Blanc P., Barot F., Braibant G., Buschaert S., Crouzet C., Gautier A., Girard J. P., Jacquot E., Lassin A., Negrel G., Tournassat C., Vinsot A. and Altmann S. (2006) Modeling the porewater chemistry of the Callovo-Oxfordian formation at a regional scale. *C. R. Geosci.* **338**(12–13), 917–930.

Gonçalvès J., Rousseau-Gueutin P. and Revil A. (2007) Introducing interacting diffuse layers in TLM calculations: a reappraisal of the influence of the pore size on the swelling pressure and the

osmotic efficiency of compacted bentonites. *J. Colloid Interface Sci.* **316**, 92–99.

Gueutin P., Altmann S., Gonçalvès J., Cosenza P. and Violette S. (2007) Osmotic interpretation of overpressures from monovalent based triple layer model, in the Callovo-Oxfordian at the Bure site. *Phys. Chem. Earth* **32**, 434–440.

Hunter R. J. (1981) *Zeta Potential in Colloid Science: Principles and Applications*. Academic Press, New York.

Jacquot E. (2002) Composition des eaux interstitielles des argilites du Callovo-Oxfordien non perturbées: état de la modélisation à Juillet 2002. ANDRA Report D NT ASTR 02-041.

Kim H., Suk T., Park S. and Lee C. (1993) Diffusivities for ions through compacted Na-bentonite with varying dry bulk density. *Waste Manag.* **13**, 303–308.

Leroy P. and Revil A. (2004) A triple-layer model of the surface electrochemical properties of clay minerals. *J. Colloid Interface Sci.* **270**(2), 371–380.

Leroy P., Revil A. and Coelho D. (2006) Diffusion of ionic species in bentonite. *J. Colloid Interface Sci.* **296**(1), 248–255.

Leroy P., Revil A., Altmann S. and Tournassat C. (2007) Modeling the composition of the pore water in a clay-rock geological formation (Callovo-Oxfordian, France). *Geochim. Cosmochim. Acta* **71**(5), 1087–1097. doi:10.1016/j.gca.2006.11.009.

Leroy P. and Revil A. (2008) Spectral induced polarization of clays and clay-rocks. *J. Geophys. Res.*

Leroy P., Revil A., Kemna A., Cosenza P. and Ghorbani A. (2008) Complex conductivity of water-saturated packs of glass beads. *J. Colloid Interface Sci.* **321**, 103–117.

Limousin G., Gaudet J.-P., Charlet L., Szenknect S., Barthès V. and Krimissa M. (2007) Sorption isotherms: a review on physical bases, modeling and measurement. *Appl. Geochem.* **22**, 249–275.

Linde N., Jougnot D., Revil A., Matthäi S., Arora T., Renard D. and Doussan C. (2007) Streaming current generation in two phase flow conditions. *Geophys. Res. Lett.* **34**, L03306. doi:10.1029/2006GL028878.

Malusis M. A., Shackelford C. D. and Olsen H. W. (2003) Flow and transport through clay membrane barriers. *Eng. Geol.* **70**, 235–248.

Melkior T. (1999) Etude méthodologique de la diffusion de cations interagissants dans des argiles. Ph.D. Thesis, Ecole Centrale de Paris.

Melkior T., Mourzagh D., Yahiaoui S., Thoby D., Alberto J. C., Brouard C. and Michau N. (2004) Diffusion of an alkaline fluid through clayey barriers and its effect on the diffusion properties of some chemical species. *Appl. Clay Sci.* **26**, 99–107.

Melkior T., Yahiaoui S., Motellier S., Thoby D. and Tevissen E. (2005) Cesium sorption and diffusion in Bure mudrock samples. *Appl. Clay Sci.* **29**, 172–186.

Melkior T., Yahiaoui S., Thoby D., Motellier S. and Barthes V. (2007) Diffusion coefficients of alkaline cations in Bure mudrock. *Phys. Chem. Earth* **32**, 453–462.

Mendelson K. S. and Cohen M. H. (1982) The effect of grain anisotropy on the electrical properties of sedimentary rocks. *Geophysics* **47**, 257–263.

Meyer K. H. and Sievers J. F. (1936) La perméabilité des membranes. I. Théorie de la perméabilité ionique. *Helv. Chem. Acta* **19**, 649.

Molera M. and Eriksen T. (2002) Diffusion of $^{22}Na^{+}$, $^{85}Sr^{2+}$, $^{134}Cs^{+}$ and $^{57}Co^{2+}$ in bentonite clay compacted to different densities: experiments and modeling. *Radiochim. Acta* **90**, 753–760.

Muurinen A., Penttilä-Hiltunen P. and Uusheimo K. (1988) Diffusion of chloride and uranium in compacted sodium bentonite. In *Scientific Basis of Nuclear waste Management XII* (eds. W. Lutze and R. C. Erwing). Materials Research Society, Pittsburg, PA, pp. 743–748.

Muurinen A. (1994) Diffusion of anions and cations in compacted sodium bentonite. VTT Publication 168, Espoo Technical Centre, Finland.

Ochs M., Lothenbach B., Wanner H., Sato H. and Yui M. (2001) An integrated sorption–diffusion model for the calculation of consistent distribution and diffusion coefficients in compacted bentonite. *J. Contam. Hydrol.* **47**, 283–296.

Parkhurst D. L. and Appelo C. A. J. (1999) User's guide to PHREEQC (version 2)—a computer program for speciation, batch-reaction, one-dimensional transport, and inverse geochemical calculations. US Geological Survey Water-Resources Investigations Report 99-4259.

Patriarche D., Ledoux E., Michelot J.-L., Simon-Coincon R. and Savoye S. (2004) Diffusion as the main process for mass transport in very low water content argillites. 2. Fluid flow and mass transport modeling. *Water Resour. Res.* **40**(1), W01517.

Revil A., Cathles L. M., Losh S. and Nunn J. A. (1998) Electrical conductivity in shaly sands with geophysical applications. *J. Geophys. Res.* **103**, 23,925–23,936.

Revil A. (1999) Ionic diffusivity, electrical conductivity, membrane and thermoelectric potentials in colloids and granular porous media: a unified model. *J. Colloid Interface Sci.* **212**, 503–522.

Revil A., Hermitte D., Spangenberg E. and Cochémé J. J. (2002) Electrical properties of zeolitized volcaniclastic materials. *J. Geophys. Res.* **107**(B8), 2168. doi:10.1029/2001JB000599.

Revil A. and Leroy P. (2004) Governing equations for ionic transport in porous shales. *J. Geophys. Res.* **109**, B03208. doi:10.1029/2003JB002755.

Revil A., Leroy P. and Titov K. (2005) Characterization of transport properties of argillaceous sediments. Application to the Callovo-Oxfordian Argillite. *J. Geophys. Res.* **110**, B06202. doi:10.1029/2004JB003442.

Revil A. and Linde N. (2006) Chemico-electromechanical coupling in microporous media. *J. Colloid Interface Sci.* **302**, 682–694.

Revil A., Linde N., Cerepi A., Jougnot D., Matthäi S. and Finsterle S. (2007) Electrokinetic coupling in unsaturated porous media. *J. Colloid Interface Sci.* **313**(1), 315–327. doi:10.1016/j.jcis.2007.03.037.

Revil A. (2007) Thermodynamics of transport of ions and water in charged and deformable porous media. *J. Colloid Interface Sci.* **307**(1), 254–264.

Revil A. and Jougnot D. (2008) Diffusion of ions in unsaturated porous materials. *J. Colloid Interface Sci.* **319**(1), 226–235. doi:10.1016/j.jcis.2007.10.041.

Sato H., Yui M. and Yoshikawa H. (1995) Diffusion behavior for Se and Zr in sodium-bentonite. *Mater. Res. Soc. Symp. Proc.* **353**, 269–276.

Steefel C. I., Carroll S. A., Zhao P. and Roberts S. (2003) Cesium migration in Hanford sediment: a multi-site cation exchange model based on laboratory transport experiments. *J. Contam. Hydrol.* **67**, 219–246.

Steefel C. I., DePaolo D. and Lichtner P. C. (2005) Reactive transport modeling: an essential tool and a new research approach for the Earth sciences. *Earth Planet. Sci. Lett.* **240**, 539–558.

Teorell T. (1935) An attempt to formulate a quantitative theory of membrane permeability. *Proc. Soc. Exp. Biol. Med.* **33**, 282.

Tikhonov A. N. (1963) Resolution of ill-posed problems and the regularization method (in Russian). *Dokl. Akad. Nauk SSSR* **151**, 501–504.

Van Brakel J. and Heertjes P. M. (1974) Analysis of diffusion in macroporous media in terms of a porosity, a tortuosity, and a constrictivity factor. *Int. J. Heat Mass Transfer* **17**, 1093–1103.

Zachara J. M., Smith S. C., Liu C., McKinley J. P., Serne R. J. and Gassman P. L. (2002) Sorption of Cs^{+} to micaceous subsurface sediments from the Hanford site, USA. *Geochim. Cosmochim. Acta* **66**, 193–211.

Zhu C. (2003) A case against K-d based transport models: natural attenuation at a mill tailings site. *Comput. Geosci.*, 29 351–359.

Associate editor: Dimitri A. Sverjensky